CrossMark

Searching for Black Hole Candidates by LAMOST and ASAS-SN

Ling-Lin Zheng[1], Wei-Min Gu[1] , Tuan Yi[1], Jin-Bo Fu[1], Hui-Jun Mu[1] , Fan Yang[2,3], Song Wang[2] , Zhong-Rui Bai[2], Hao Sou[1],
Yu Bai[2] , Yi-Ze Dong[1,4], Hao-Tong Zhang[2], Ya-Juan Lei[2], Junfeng Wang[1] , Jianfeng Wu[1], and Jifeng Liu[2,5]

[1] Department of Astronomy, Xiamen University, Xiamen, Fujian 361005, People's Republic of China; guwm@xmu.edu.cn
[2] National Astronomical Observatories, Chinese Academy of Sciences, Beijing 100012, People's Republic of China
[3] Infrared Processing and Analysis Center, California Institute of Technology, Pasadena, CA 91125, USA
[4] Department of Physics, University of California, Davis, CA 95616, USA
[5] College of Astronomy and Space Sciences, University of Chinese Academy of Sciences, Beijing 100049, People's Republic of China

Abstract

Most dynamically confirmed stellar-mass black holes (BHs) and their candidates were originally selected from X-ray outbursts. In the present work, we search for BH candidates in the Large Sky Area Multi-Object Fiber Spectroscopic Telescope (LAMOST) survey using the spectra along with photometry from the All Sky Automated Survey for SuperNovae (ASAS-SN), where the orbital period of the binary may be revealed by the periodic light curve, such as the ellipsoidal modulation type. Our sample consists of nine binaries, where each source contains a giant star with large radial velocity variation ($\Delta V_R \gtrsim 70$ km s^{-1}) and periods known from light curves. We focus on the nine sources with long periods ($T_{ph} > 5$ days) and evaluate the mass M_2 of the optically invisible companion. Since the observed ΔV_R from only a few repeating spectroscopic observations is a lower limit of the real amplitude, the real mass M_2 can be significantly higher than the current evaluation. It is likely an efficient method to place constraints on M_2 by combining ΔV_R from LAMOST and T_{ph} from ASAS-SN, particularly by the ongoing LAMOST Medium Resolution Survey.

Unified Astronomy Thesaurus concepts: Stellar mass black holes (1611); Compact binary stars (283); Stellar photometry (1620); Radial velocity (1332); Stellar spectral types (2051)

1. Introduction

It is well known that three types of compact objects in the universe are white dwarfs, neutron stars, and black holes (BHs). Since an isolated BH does not produce electromagnetic radiation, most confirmed stellar-mass BHs and candidates were found in binaries (Remillard & McClintock 2006). For a binary system composed of a BH and an optically visible star filling its Roche lobe, the matter from the star can be accreted by the BH through the inner Lagrange point. In such cases, an accretion disk is formed and X-ray emission is produced from the disk. Thus, such a BH binary system can be detected by X-ray telescopes. However, the number of confirmed BHs and BH candidates found by this method is less than a hundred (Corral-Santana et al. 2016), which is far below the number of BHs that are thought to exist in our Galaxy (e.g., Brown & Bethe 1994).

New methods are required to search for more BH candidates. For binaries with unknown orbital periods, Gu et al. (2019) proposed a method to search for BH candidates from optical observations. The method is based on the assumption that the radius R_1 of the optically visible star is no more than the corresponding Roche-lobe radius R_{L1}. On the other hand, once the orbital period P_{orb} can be derived (such as being revealed by the periodic light curves), we can obtain the well-known mass function (refer to Equation (5) in Section 3.2) and therefore place better constraints on the optically invisible companion. In a BH binary, if the ratio R_1/R_{L1} is not far below unity, the companion may be pulled into a waterdrop shape due to the strong gravity of the BH. The deformed star will present a periodic light curve with the ellipsoidal modulation (Morris 1985). Thus, the light curve may reveal the orbital period P_{orb} of the system and is helpful to the constraints of M_2.

The Large Sky Area Multi-Object Fiber Spectroscopic Telescope (LAMOST) provides nearly 10 million stellar spectra in the Data Release 6 and about 480 thousand low-resolution stellar spectra in the Data Release 7. Furthermore, it has radial velocity to a precision of better than 5 km s^{-1} (Deng et al. 2012). We can derive many key parameters (T_{eff}, $\log g$, and [Fe/H]) and heliocentric radial velocity V_R from the spectra (Zong et al. 2018). In addition, the All Sky Automated Survey for Super-Novae (ASAS-SN) monitors the entire visible sky to a depth of $V \lesssim 17$ mag for bright supernovae and other transients. For instance, the ASAS-SN V-band light curves of around 412 thousand variable stars were studied by Jayasinghe et al. (2019).

The aim of this paper is to introduce the method to search for BH candidates by combining the LAMOST spectra and the ASAS-SN photometry. We will introduce the data selection from LAMOST in Section 2. The analyses and results of our sample are shown in Section 3. Conclusions and discussion are presented in Section 4.

2. Data Selection

The present work focuses on binaries with a giant star. For a giant star, the variation of radial velocity in the same night is usually negligible due to its large size, and therefore its orbital period is relatively long. We select a sample of binaries containing a giant star from LAMOST Data Release 6 and LAMOST Data Release 7 with the following criteria:

$$\begin{cases} S/N_{(g)} > 10 \text{ (signal-to-noise in the } g \text{ band)}, \\ 3800 \text{ K} < T_{eff} < 5300 \text{ K}, \\ 1.5 \text{ dex} < \log g < 3.5 \text{ dex}, \\ -1.0 \text{ dex} < [Fe/H] < 0.5 \text{ dex}, \\ \text{single-lined spectra only.} \end{cases}$$

Furthermore, the selected sources have at least two-night exposures in the LAMOST database, and the largest radial

velocity variation $\Delta V_R \gtrsim 70\,\mathrm{km\,s^{-1}}$. Consequently, we obtain a sample of 43 single-lined binaries. In addition, the sources without *Gaia* parallax or with negative parallax have been removed (Jayasinghe et al. 2019; Ziaali et al. 2019). We cross-match the sources with the ASAS-SN Sky Patrol[6] database (Shappee et al. 2014; Kochanek et al. 2017), and therefore we derive a sample of 17 binaries with periods longer than 5 days (the reason is given in the fourth paragraph of Section 3.1). We refer to the signal-to-noise ratio (S/N) in Equation (6) from Hartman & Bakos (2016) to measure the significance for peaks identified in the periodogram. Finally, we obtain nine sources with $\mathrm{S/N}(T_{ph}) > 30$ as our sample, which are shown in Table 1. We also cross-match our sample with simbad in 5″, and find that only source number 3 has X-ray information (refer to Section 3.1).

Since the sources in our sample are all with single-lined spectra, the unseen object in a binary is therefore either a compact object or a much fainter star, roughly speaking, less than 10% of the luminosity of the observed giant star. The luminosity is shown in column 14 of Table 1, which is calculated by the apparent magnitude from UCAC4 and the parallax from *Gaia* DR2, where the bolometric correction and extinction have been taken into consideration. It is seen from Table 1 that the luminosity of these sources is less than 100 solar luminosities. If the unseen object is a main-sequence star or a subgiant star with 3 solar masses, it will be more than 30 solar luminosities. Thus, it ought to be observed and the corresponding spectra of the binary should not be the single-lined type. Thus, once $M_2 > 3M_\odot$ is matched, the unseen object has a high possibility of being a BH. In this work, we manage to search for BH candidates following this spirit. We would point out another possibility that the system is a triple system. For example, if the system consists of a giant star and a pair of 1.5 solar mass stars in a close binary, then the total luminosity of the pair of stars is around 10 solar luminosities, and therefore may be optically invisible.

3. Results

3.1. Period Analyses

The Lomb–Scargle method (Lomb 1976; Scargle 1981) is a useful statistical tool to extract periodic signals in unevenly spaced data. This method can reflect the intensity of the captured periodic signal on the power peaks. The Lomb–Scargle periodogram is calculated and the period corresponding to the highest power was extracted. Then light curves can be folded with the retrieved periods. We searched for the periods for the sources in our sample, and five of them (source numbers 1–3, 7, and 8) have been investigated by Gu et al. (2019) without any information of the period. The folded light curves for the nine sources are shown in Figure 1. As mentioned in Section 2, only source number 3 was known as a faint X-ray source according to the *ROSAT* observations (Voges et al. 2000). The light curve of this source in Figure 1 shows that it may have two possibilities. One is an eclipsing binary caused by an accretion disk, which coincides with the X-ray observations. The other possibility is an eclipsing binary of the Algol type where the X-ray emission is related to an active star. From the shape of light curves, the other eight sources in our sample may be either the ellipsoidal modulation type or the

eclipsing binary type. We would stress that, for both of these two mechanisms, the periodic variability can reveal the orbital period. Thus, we can evaluate the mass of the unseen object using the orbital period.

We compare our derived period based on the Lomb–Scargle algorithm with that given by ASAS-SN. We found that our results are identical to that from the ASAS-SN website, except for source number 2. The photometric period (55.1046 days) from the ASAS-SN website for this source is exactly twice of ours (27.5509 days). In our opinion, the different periods may result from different folding algorithms. For this source, we adopt our period in the following analyses.

Even though the shape of folded light curves may indicate that the photometric period T_{ph} is identical with the orbital period P_{orb}, some analyses are required to confirm that. In a binary, the relation between the separation a and P_{orb} takes the form of

$$\frac{G(M_1 + M_2)}{a^3} = \frac{4\pi^2}{P_{orb}^2}. \tag{1}$$

In addition, the Roche-lobe radius of the optically visible star R_{L1} can be expressed as (Paczyński 1971)

$$\frac{R_{L1}}{a} = 0.462\left(\frac{M_1}{M_1 + M_2}\right)^{1/3}. \tag{2}$$

Based on the reasonable assumption that the radius of the giant star is no larger than the Roche-lobe radius, i.e., $R_l \leqslant R_{L1}$ (Gu et al. 2019), and by combining Equations (1) and (2), the following inequality can be derived:

$$P_{orb} \geqslant 2\pi\left[\frac{(R_l/0.462)^3}{GM_1}\right]^{1/2}. \tag{3}$$

Thus, there exists a lower limit for the orbital period once R_1 and M_1 (or simply the mass density ρ_1) is derived:

$$P_{orb}^{min} = 0.369\,(\rho_1/\rho_\odot)^{-1/2}\,\text{days}, \tag{4}$$

where $\rho_\odot$ is the solar density.

As indicated by Equation (4), if the optically visible star is of main sequence, the orbital period can be less than one day, which agrees well with most confirmed BHs in low-mass X-ray binaries. In this work, however, we focus on the cases in which the companion is a late-type giant star, such as a red giant. For instance, given $M_1 = M_\odot$ and $R_1 = 10\,R_\odot$, Equation (4) results in $P_{orb}^{min} \approx 11.7$ days. That is why we have focused on the nine sources with $T_{ph} > 5$ days. Otherwise, the photometric period T_{ph} is unlikely the orbital period P_{orb}.

For the sources in our sample, apparent periodic variability (0.1 ~ 0.5 mag) has been observed. If the periodic variability is related to the ellipsoidal modulation, then the radius of an optically visible star cannot be far below the corresponding Roche-lobe radius. Consequently, the period T_{ph} should not be far beyond P_{orb}^{min}. Figure 2 shows the consistency of the photometric period and the orbital period. A comparison of the observations with our analyses is shown in Figure 2, where the analytic P_{orb}^{min} for $R_1 = R_{L1}$ (solid line) is calculated by Equation (4). In addition, since the giant star may not fill its Roche lobe, we also plot the analytic P_{orb} for $R_l = 0.5R_{L1}$ (dashed line). The observations for the nine sources are denoted by different symbols, where M_1 and R_1 are derived by the stellar evolution model, as mentioned in Table 1. It is seen from

Table 1
Parameters for the Sources in Our Sample

No.	R.A.	Decl.	T_{ph} (days)	S/N(T_{ph})	$T_{eff,L}$ (K)	log g (dex)	[Fe/H] (dex)	N_{obs}	ΔV_R (km s^{-1})	ϖ (mas)	Vmag (mag)	Kmag (mag)	L ($L_\odot$)	R_1 ($R_\odot$)	M_1 ($M_\odot$)	M_2 ($M_\odot$)
(1)	(2)	(3)	(4)	(5)	(6)	(7)	(8)	(9)	(10)	(11)	(12)	(13)	(14)	(15)	(16)	(17)
1	0.839201575	38.51855052	11.8608	118.56	4696 ± 57	2.65 ± 0.09	−0.25 ± 0.05	3	93.5 ± 5.6	0.505 ± 0.043	12.736	9.952	50.176	$8.1^{+1.5}_{-0.8}$	$1.1^{+0.3}_{-0.1}$	$0.9^{+0.2}_{-0.1}$
2[a]	3.887105349	38.68886824	27.5509	116.33	4301 ± 44	1.95 ± 0.07	−0.47 ± 0.04	4	83.7 ± 6.2	0.379 ± 0.032	12.665	9.641	91.627	$17.8^{+0.6}$	$0.9^{+1.5}$	$1.1^{+0.9}$
3	74.05325351	54.00589535	5.2085	55.65	4769 ± 106	2.68 ± 0.17	−0.31 ± 0.10	6	127.2 ± 7.8	1.068 ± 0.034	12.784	9.004	31.245	$7.8^{+3.5}_{-0.7}$	$1.1^{+0.7}_{-0.2}$	$1.0^{+0.4}_{-0.2}$
4[a]	82.31076394	42.09587217	9.6409	39.49	4700 ± 98	2.97 ± 0.15	−0.36 ± 0.09	4	70.5 ± 6.7	1.398 ± 0.048	12.727	9.941	6.774	$5.1^{+2.8}$	$0.9^{+0.4}$	$0.5^{+0.2}$
5	93.81977494	22.11031808	15.5915	32.38	4796 ± 25	2.43 ± 0.04	−0.47 ± 0.02	2	78.1 ± 5.6	1.090 ± 0.072	11.362	8.051	77.445	$12.0^{+3.3}_{-3.4}$	$1.4^{+0.6}_{-0.5}$	$0.9^{+0.3}_{-0.2}$
6	102.0930387	21.82487008	7.1848	37.92	5093 ± 29	3.11 ± 0.05	−0.27 ± 0.03	2	78.1 ± 6.6	0.539 ± 0.042	12.920	10.231	42.086	$6.0^{+0.8}_{-0.8}$	$1.7^{+0.2}_{-0.3}$	$0.7^{+0.2}_{-0.1}$
7	111.3363737	28.06745981	28.0117	42.72	4833 ± 188	2.75 ± 0.30	−0.23 ± 0.18	6	85.1 ± 7.6	0.152 ± 0.032	14.698	12.075	82.412	$8.7^{+2.8}_{-1.9}$	$1.5^{+0.6}_{-0.4}$	$1.4^{+0.5}_{-0.3}$
8[a]	169.1246518	55.72840217	46.8920	74.31	4191 ± 102	1.82 ± 0.16	−0.75 ± 0.10	3	97.8 ± 5.8	1.086 ± 0.031	10.638	7.377	82.415	$20.8^{+8.1}$	$0.9^{+0.5}$	$1.9^{+0.6}$
9	325.3386324	28.4225968	17.4856	40.81	4770 ± 78	2.51 ± 0.12	−0.15 ± 0.07	2	73.2 ± 5.2	1.063 ± 0.036	10.675	8.036	67.864	$10.8^{+4.1}_{-0.2}$	$1.9^{+0.6}_{-0.7}$	$1.1^{+0.3}_{-0.4}$

Note.

[a] The lower limit of M_1 or R_1 cannot be well estimated from the PARSEC model. Column (1): number of the source; column (2): R.A. (J2000); column (3): decl. (J2000); column (4): folded period from the ASAS-SN photometry; column (5): significance of the periodogram; column (6): effective temperature from LAMOST; column (7): surface gravity from LAMOST; column (8): metallicity from LAMOST; column (9): times of observations; column (10): observed largest variation of radial velocity; column (11): parallax from *Gaia*; column (12): *V*-band magnitude from UCAC4; column (13): *K*-band magnitude from UCAC4; column (14): luminosity calculated by the apparent magnitude from UCAC4 and the parallax from *Gaia* DR2; column (15): radius of the giant star from the PARSEC model; column (16): mass of the giant star from the PARSEC model; and column (17): mass of the invisible star for "$i = 60°$, $K_1 = \Delta V_R/2$, and $P_{orb} = T_{ph}$."
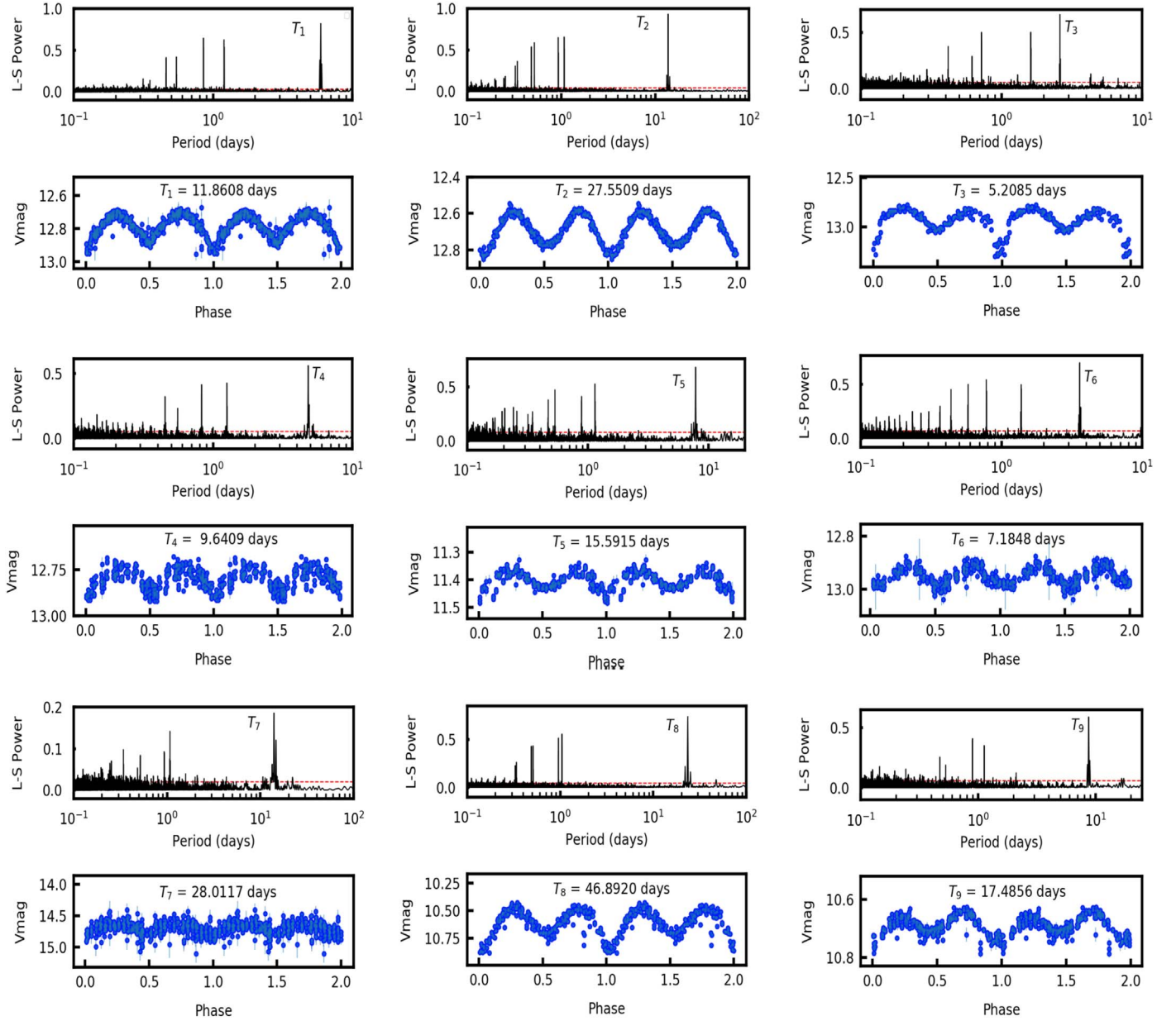
Figure 1. Light curves of the nine sources in Table 1 folded by the Lomb–Scargle algorithm, where the period of variability is shown in each panel.

Figure 2 that all nine sources are well located around the solid line or between the solid line and the dashed line, which indicates that the relation $P_{orb} = T_{ph}$ is quite reasonable. As a consequence, we can place better constraints on the mass M_2 with the values of P_{orb}.

3.2. Mass Measurement

We evaluate the mass M_1 of the nine sources in our sample by the PARSEC model[7] (Marigo et al. 2008; Bressan et al. 2012), and measure the mass of the optically invisible companion by the equation of mass function. The well-known mass function for M_2 takes the form (Remillard & McClintock 2006)

$$f(M_2) \equiv \frac{M_2 \sin^3 i}{(1 + q)^2} = \frac{K_1^3 P_{orb}}{2\pi G}, \quad (5)$$

where $K_1 \geqslant \Delta V_R/2$ is the semi-amplitude of the giant star and the mass ratio is defined as $q \equiv M_1/M_2$. In the above equation, once K_1 and P_{orb} are given, the mass function $f(M_2)$ can be obtained, and it is certain that $M_2 > f(M_2)$. In addition, if M_1 can be derived from the spectra and $\sin i$ is provided, then M_2 can be well constrained. Referring to the inclination angle of most BH binaries in Corral-Santana et al. (2016), we assume a typical inclination angle of $i = 60°$ in this work.

As shown in Table 1, M_1 of most sources are in the range of $1\,M_\odot < M_1 < 2\,M_\odot$. If $M_2 > 3M_\odot$ can be matched, the source can be regarded as a BH candidate. However, it is not easy to directly satisfy such a condition. On the other hand, if $M_2 > M_1$ can be matched, according to the rule of stellar evolution, the optically invisible star is likely to be a compact object (except for the Algol case, see below). Thus, we plot four theoretical lines in Figure 3 (from bottom to top) corresponding to $(M_1 = 1\,M_\odot, \ M_2 = M_1)$, $(M_1 = 2\,M_\odot,$
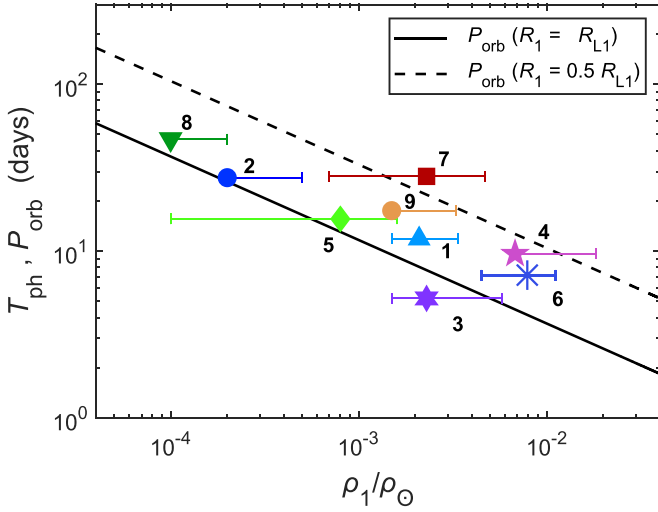
4

Figure 2. Comparison of the analytic orbital period P_{orb} (lines) with the observational variability period T_{ph} (symbols). The solid line represents the lower limit P_{orb}^{min} calculated by Equation (4), where the giant star fills its Roche lobe ($R_1 = R_{L1}$). The dashed line corresponds to a case in which the Roche lobe is not filled, with $R_1 = 0.5R_{L1}$.

Figure 3. Comparison between analyses and observations in the K_1-T_{ph} diagram, where the semi-amplitude K_1 is no less than half of the observed maximal variation in a few repeating observations ($K_1 \geqslant \Delta V_R/2$).

$M_2 = M_1$), ($M_1 = 2\,M_\odot$, $M_2 = 3\,M_\odot$), and ($M_1 = 1\,M_\odot$, $M_2 = 3\,M_\odot$), respectively.

It is seen from Figure 3 that, there is no source above or even in the upper shaded region, which means that there is no strong BH candidate according to the current observations. On the other hand, source number 8 is located well above the green shaded region, and close to the blue shaded region. Even under the extreme case with the inclination angle is $i = 90°$, we also derive $M_2 > M_1$. Hence source number 8 is probably a compact object. Whether or not it is a BH requires follow-up spectroscopic observations to obtain the radial velocity curve. However, we would point out that there exist some binaries like Algol, in which the lower mass star is more evolved than its companion. Thus, mass exchange can allow $M_2 > M_1$ with the more massive star being on the main sequence. In other words, the condition $M_2 > M_1$ may imply a compact star but is not a sufficient condition. In addition, most sources in Table 1 have only two or three observations, and the semi-amplitude of radial velocity K_1 may be significantly larger than the current $\Delta V_R/2$. Thus, it is quite possible for the mass M_2 to be significantly higher than the current evaluation. We therefore use the black arrows in Figure 3 to show such an increase possibility.

4. Conclusions and Discussion

In this work, we have proposed a method to search for stellar-mass BH candidates by including the LAMOST spectra and the ASAS-SN photometry, where the orbital period P_{orb} may be revealed by the periodic light curve. We have obtained a sample of nine single-lined spectroscopic binaries containing a giant star with a large radial velocity variation of $\Delta V_R \gtrsim 70\,km\,s^{-1}$, and the photometric period of the sources satisfy $T_{ph} > 5$ days. Moreover, based on the relation $R_1 \leqslant R_{L1}$, we have checked that T_{ph} and P_{orb} are likely identical for the sources in our sample. As a consequence, the mass M_2 can be better constrained. We have shown that source number 8 is likely to be a compact object. It is worth follow-up spectroscopic observations to check whether it is a BH. Moreover, for
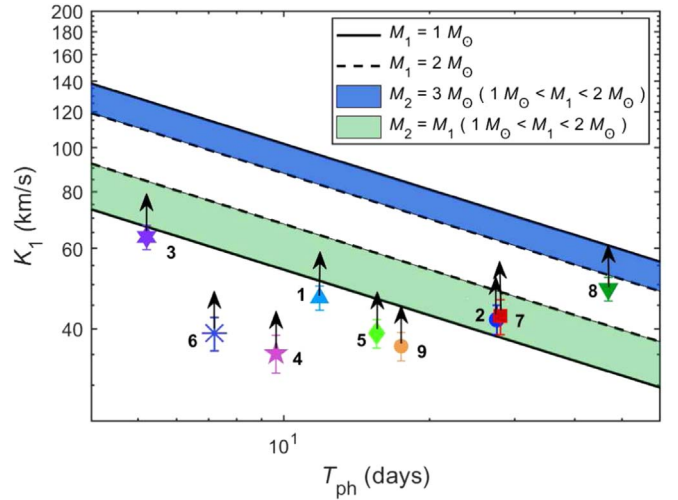
the other sources, the real mass M_2 can be significantly higher than the current evaluation. Thus, they are also potential BH candidates. In our opinion, it is an efficient method to constrain M_2 by combining the LAMOST spectra and the ASAS-SN photometry.

In this work, we have focused on the giant companion. In fact, our method is also valid for the main-sequence star case. Normally, the orbital period P_{orb} of a main-sequence star is significantly shorter (less than one day, as implied by Equation (4)) for the ellipsoidal modulation type. In such case, the radial velocity variation in the same night can provide crucial information. Thus, once the single exposure spectra of LAMOST are released, many more BH candidates can be found through our method. On the other hand, the LAMOST Medium Resolution Survey will provide more accurate radial velocity and more repeating exposures (around 60 exposures for a source in the time-domain spectroscopic survey), which enable us to derive a clear radial velocity curve and to make a better constraint on the mass of candidates.

The sources in our sample are binaries with relatively long orbital periods ($5 \sim 47$ days). However, the *Gaia* DR2 solution has assumed a single-star model and has mistaken the binary motion itself as part of the parallax, which may result in systematic errors for the parallax and distance. Whether the real parallaxes are larger or smaller than the current values is related to the observational times. For the cases with adequate observations by *Gaia*, the real parallaxes will be smaller. On the contrary, for the cases with inadequate observations, the results will be quite uncertain. In DR3, the non-single-star model will be considered in the data analysis. In the full release of the nominal mission, the catalog will provide all available variable-star and non-single-star solutions.

ORCID iDs

Wei-Min Gu ● https://orcid.org/0000-0003-3137-1851
Hui-Jun Mu ● https://orcid.org/0000-0001-6589-2220
Song Wang ● https://orcid.org/0000-0003-3116-5038
Yu Bai ● https://orcid.org/0000-0002-4740-3857
Junfeng Wang ● https://orcid.org/0000-0003-4874-0369

References

Bressan, A., Marigo, P., Girardi, L., et al. 2012, MNRAS, 427, 127
Brown, G. E., & Bethe, H. A. 1994, ApJ, 423, 659
Corral-Santana, J. M., Casares, J., Muñoz-Darias, T., et al. 2016, A&A, 587, A61
Deng, L.-C., Newberg, H. J., Liu, C., et al. 2012, RAA, 12, 735
Gu, W.-M., Mu, H.-J., Fu, J.-B., et al. 2019, ApJL, 872, L20
Hartman, J. D., & Bakos, G. Á 2016, A&C, 17, 1
Jayasinghe, T., Stanek, K. Z., Kochanek, C. S., et al. 2019, MNRAS, 486, 1907
Kochanek, C. S., Shappee, B. J., Stanek, K. Z., et al. 2017, PASP, 129, 104502
Lomb, N. R. 1976, Ap&SS, 39, 447
Marigo, P., Girardi, L., Bressan, A., et al. 2008, A&A, 482, 883
Morris, S. L. 1985, ApJ, 295, 143
Paczyński, B. 1971, ARA&A, 9, 183
Remillard, R. A., & McClintock, J. E. 2006, ARA&A, 44, 49
Scargle, J. D. 1981, ApJS, 45, 1
Shakura, N. I., & Sunyaev, R. A. 1973, A&A, 24, 337
Shappee, B. J., Prieto, J. L., Grupe, D., et al. 2014, ApJ, 788, 48
Voges, W., Aschenbach, B., Boller, T., et al. 2000, IAUC, 7432, 3
Ziaali, E., Bedding, T. R., Murphy, S. J., et al. 2019, MNRAS, 486, 4348
Zong, W., Fu, J.-N., De Cat, P., et al. 2018, ApJS, 238, 30